bioresources.cnr.ncsu.edu

Impact of Drying Temperature on the Physicochemical and Functional Properties of Butterfly Pea Flower Powder

Jagamohan Meher,[a] Gnaniar Kalusuraman,[b,]* Niraj Kumar Dewangan,[c] Rajanandini Meher,[d] Senthilkumar Krishnasamy,[e,]* Santosh Kumar Sahu ⓘD,[f,]* Jayant Giri,[g,h,i] and Mohammad Kanan[j,k,]*

Butterfly pea flower (BPF) powder, which is rich in bioactive compounds, was evaluated for the impact of various drying methods on its solubility, physical properties, and chemical composition. Four drying methods were used: thermal drying at 50 °C, 60 °C, 70 °C, and natural sun drying. The powders were assessed for solubility time, hygroscopicity, density, flowability, and chemical stability using scanning electron microscopy (SEM), X-ray diffraction (XRD), and Fourier transform infrared (FTIR). Solubility times ranged from 148 to 162 s, with no significant differences. The 70 °C dried sample (Sample C) had the fastest dissolution rate and highest hygroscopicity. Total phenolic and anthocyanin contents increased with temperature, peaking in sun-dried samples (Sample D). Density measurements showed Sample C had the highest bulk density and optimal flowability, while Sample D had superior water holding capacity. The SEM analysis revealed morphological differences, with Sample A showing a smooth surface and Sample C exhibiting significant particle disintegration. The XRD analysis showed that Sample C had the highest crystallinity. The FTIR analysis confirmed the stability of key functional groups, with sun-dried samples retaining phenolic compounds. These findings suggest drying methods can optimize BPF powder's properties, enhancing its bioactivity for health applications.

Contact information: a: Krishi Vigyan Kendra Kalahandi, Odisha University of Agriculture and Technology, Bhubaneswar, Odisha, India; b: Department of Mechanical Engineering, Kalasalingam Academy of Research and Education, Krishnankoil, Krishnankoil 626126, Srivilliputhur, Tamilnadu, India; c: Department of Mechatronics, Manipal Institute of Technology, Manipal Academy of Higher Education, Manipal 576 104, India; d: Department of Biotechnology, Kalasalingam Academy of Research and Education, Krishnankoil 626126, Srivilliputhur, Tamilnadu, India; e: Department of Mechanical Engineering, PSG Institute of Technology and Applied Research, Coimbatore 641062, Tamilnadu, India; f: School of Mechanical Engineering, VIT-AP University, Besides A.P. Secretariat, Amaravati 522237, Andhra Pradesh, India; g: Department of Mechanical Engineering, Yeshwantrao Chavan College of Engineering, Nagpur, India; h: Division of Research and Development, Lovely Professional University, Phagwara, India; i: Centre for Research Impact & Outcome, Chitkara University Institute of Engineering and Technology, Chitkara University, Rajpura, 140401, Punjab, India; j: Department of Industrial Engineering, College of Engineering, University of Business and Technology, Jeddah 21448, Saudi Arabia; k: Department of Mechanical Engineering, College of Engineering, Zarqa University, Zarqa; *Corresponding authors: kalusunrk@gmail.com; kmsenthilkumar@gmail.com; sksahumech@gmail.com; m.kannan@ubt.edu.sa

---

INTRODUCTION

Rising consumer interest in natural and health-promoting products has renewed focus on traditional and herbal remedies, particularly those derived from plants that have well-established therapeutic benefits. *Clitoria ternatea*, commonly known as butterfly pea, has garnered significant attention for its diverse and documented health benefits. This herbaceous plant, a member of the Fabaceae family, is noted for its vibrant deep blue flowers, which are used to make the popular herbal infusion known as "blue tea" (Oguis *et al.* 2019; Barman and Kar 2023). Native to Asia and the Americas, butterfly pea demonstrates impressive adaptability to various semi-arid and sub-humid climates across Asia, Africa, and Australia, highlighting due to its potential for widespread cultivation and application in diverse environmental conditions. Blue tea, prepared from dried butterfly pea flowers, is distinguished not only by its striking color but also by its rich antioxidant content, particularly anthocyanins, which confer both the deep blue hue and associated health benefits. These benefits include digestive support, weight management, improved skin and hair health, and potential anti-cancer effects (Oguis *et al.* 2019; Vidana Gamage *et al.* 2021). Despite these advantages, global consumption of blue tea remains relatively low, which may be attributed to inconsistent quality resulting from variations in drying and preparation processes. Research indicates that the drying method significantly affects the retention of bioactive compounds, such as anthocyanins, which are sensitive to factors including temperature, light, and pH. The degradation of anthocyanins due to heat exposure can lead to color loss and reduced antioxidant activity, underscoring the need for appropriate drying techniques to preserve these compounds during the processing of BPF powder (Enaru *et al.* 2021; Belwal *et al.* 2022).

The production of instant powders from BPF is advantageous due to their practicality, extended shelf life, and ease of use (Marpaung *et al.* 2020). However, the quality of these powders, including color, flavor, and nutritional content, is highly dependent on the drying process. For instance, spray drying, which is commonly used in the food industry, can produce fine, stable powders but requires precise control of drying parameters to avoid the loss of heat-sensitive nutrients (Ziaee *et al.* 2023). This study aims to evaluate the effects of various drying temperatures on the physical, chemical, and functional properties of BPF powder. Through examining parameters, such as crystallinity, particle morphology, and color stability, the research seeks to identify optimal drying conditions that maximize the retention of anthocyanins and other beneficial compounds. Previous studies have highlighted those different drying methods, such as freeze-drying, vacuum drying, and spray drying, each have unique advantages and challenges in preserving the quality of natural products (Hariadi *et al.* 2024).

The objective of this research was to contribute to the existing knowledge on BPF processing by identifying the most effective drying methods for preserving the functional and nutritional qualities of BPF powder. Through comparing the impact of different drying temperatures on the powder's physical properties and bioactive content, this study aimed to optimize preparation methods for BPF. The findings are intended to support the broader adoption of BPF products by ensuring consistent quality and maximizing the health benefits of this remarkable plant, aligning with the current trend towards natural and functional foods.

EXPERIMENTAL

Materials Collection

The BPF (*Clitoria ternatea*) samples were meticulously sourced from Kalasalingam University Farm in Sriviliputhur, Tamil Nadu, India. To maximize bioactive compound content, the samples were harvested at full bloom. After harvesting, the flowers were promptly separated from their stems, and only intact specimens were selected for further processing. The flowers were uniformly chopped into smaller pieces approximately 2 cm in length using a stainless-steel knife to maintain consistency during the subsequent drying process. After oven drying at a controlled temperature, the resulting BPF powder was stored in airtight containers and kept in a dark environment to protect against moisture and light-induced degradation of bioactive compounds. Figure 1 shows the step-by-step procedure of processing the BPF powder.
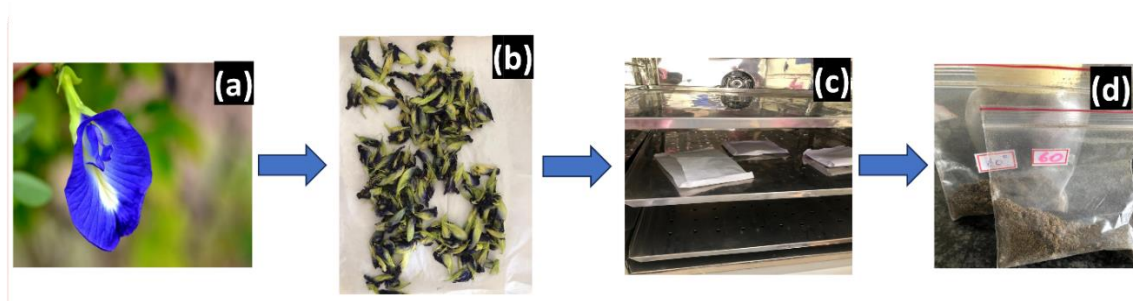

Fig. 1. Step-by-step processing stages of BPF (*Clitoria ternatea*): (a) harvesting of BPF samples, (b) chopping into uniform pieces (2 cm), (c) oven drying at controlled temperature, and (d) storage of the final BPF powder in airtight containers

Drying and Powdering of BPF

In this study, two primary drying methods were employed for BPF: (i) shade drying, and (ii) oven drying. Additionally, a sun-dried sample was prepared and used as a control for comparative analysis with the oven-dried samples. Initially, 500 g of freshly harvested flowers were subjected to shade drying under ambient indoor conditions (28 to 32 °C, 65 to 70% relative humidity) for approximately 36 h. This method was chosen to preserve thermolabile compounds, as shade drying has been shown to better maintain the phytochemical integrity of plant materials compared to direct sunlight exposure (Thamkaew *et al.* 2021). The samples were placed in a well-ventilated, sheltered area, protected from direct sunlight and rain, to ensure gradual moisture reduction and prevent microbial growth.

For sun drying, a separate portion of the flowers was exposed to direct sunlight in an open but rain-protected area, with ambient temperatures ranging from 32 to 36 °C and relative humidity of 55 to 65%. Natural airflow was maintained throughout the 36-hour drying period. After shade or sun drying, a portion of the flowers was packed in butter paper for initial weight measurement, while the remainder was set aside for further drying.

The final drying phase utilized an oven dryer (Model SIBATA SD 60, Japan) at three different temperatures: 50, 60, and 70 °C, with an air velocity of 1.0 m/s. The drying process was monitored at half-hour intervals using a precision digital balance to track weight changes until the samples reached equilibrium moisture content. Each batch underwent a 90-min drying period, optimized to retain bioactive compounds as per Kadam

et al. (2012), who emphasized controlled drying temperatures for preserving plant functional properties.

After drying, the BPF were finely ground into a uniform powder, resulting in four distinct samples (Table 1). The powders were segregated according to their drying conditions and labelled accordingly. This labelling facilitated accurate comparison during subsequent analyses. The samples were stored in zip-lock bags at ambient conditions, protected from light and air to maintain herbal powder quality.

Table 1. Details of BPF Samples

Sample Details	Drying Temperature (°C)
Sample A	50
Sample B	60
Sample C	70
Sample D	Naturally sun-dried

Physiochemical Analysis
Bulk, particle, and tapped density measurements

The bulk density of the BPF was determined using the procedure described by Shenoy and Prakash (2002). A 5 g sample of BPF powder was carefully weighed and placed into a 50-mL graduated measuring cylinder. The sample was packed by tapping the cylinder gently on the bench top 10 times from a height of 5 cm to ensure uniform compaction. The final volume of the sample within the cylinder was measured, and the bulk density was calculated using Eq. 1:

$$\text{Bulk density} = \frac{\text{Mass of the powder}}{\text{The total volume of the sample after tapping}} \qquad (1)$$

Particle density was measured following the method outlined by Jinapong *et al.* (2008). In this procedure, 1 g of BPF powder was poured into a 10-mL measuring cylinder equipped with a glass stopper. To this, 5 mL of petroleum ether was added gently, and the mixture was shaken until the powder particles were fully suspended. After shaking, the wall of the cylinder was rinsed with an additional 1 mL of petroleum ether. The total volume of the petroleum ether and suspended particles was recorded. Particle density was calculated using Eq. 2:

$$\text{Particle density} = \frac{\text{Mass of the powder}}{\text{Total volume of petroleum ether and suspended particles}} \qquad (2)$$

Porosity, Hausner Ratio, and Carr Index Measurements

Porosity (ε) was then calculated using the particle density and the tapped density, as described by Jinapong *et al.* (2008). The calculation was performed using Eq. 3:

$$\varepsilon = \left[\frac{(\text{Particle density} - \text{Tap density})}{\text{Tap density}} \right] \times 100 \qquad (3)$$

The cohesion and flowability of the powders were assessed using the Hausner ratio (HR) and Carr index (CI) methods, as described by Jinapong *et al.* (2008). The Hausner ratio was calculated using Eq. 4:

$$\text{Hausner ratio (HR)} = \frac{\text{Tapped density}}{\text{Bulk density}} \qquad (4)$$

The Carr index, which indicates the flowability of the powder, was calculated using Eq. 5:

$$\text{Carr index (\%)} = \left[\frac{(\text{Tap density} - \text{Bulk density})}{\text{Tap density}}\right] \times 100 \tag{5}$$

Hydration and Adsorption Properties

Water holding capacity (WHC)

The water holding capacity (WHC) was measured using a modified method based on Zhang *et al.* (2012). A precise 0.2 g of BPF powder (M1) was dispersed in 10 mL of distilled water and transferred into a centrifuge tube (M). The tube was then placed in a water bath at 60 °C for varying durations of 10, 20, 30, 40, 50, and 60 min. After incubation, the tube was centrifuged at 2,320 rpm for 20 min. The supernatant was carefully decanted, and the sediment was then dried in an oven at 105 °C for 16 h to remove retained moisture. The dry weight of the remaining BPF powder (M2) in the tube was recorded. The WHC (g/g) was calculated using Eq. 6.

$$\text{WHC} = \frac{M_2 - (M + M_1)}{M_1} \tag{6}$$

Quantification of water solubility index

The water solubility index (WSI) was determined using the method outlined by (Yağcı and Göğüş 2008). In this procedure, 10 g of the sample were boiled in 200 mL of distilled water. The resulting solution was transferred to centrifuge tubes and centrifuged at 3000 rpm for 5 min. The supernatant was allowed to settle for 30 min. Then, 25 mL of the supernatant was transferred to pre-weighed Petri dishes and oven-dried at 105 °C for 5 h. The WSI was calculated using the Eq. 7:

$$\text{WSI(\%)} = \left(\frac{\text{Weight of dissolved solids in supernatant}}{\text{Weight of dry solids}}\right) \times 100 \tag{7}$$

Solubility time

Solubility was assessed using a modified method from Chuchird *et al.* (2024). For each sample, 1 g was added to 50 mL of warm water (approximately 70 °C) in a 250-mL beaker. The mixture was stirred continuously with a magnetic stirrer (IKA, C-MAG HS7, Germany) set at speed level 2. The solubility of the powder was determined by real-time monitoring of the time taken for the powder to completely dissolve. Each sample was tested in five replicates.

Hygroscopicity Measurement

Ten grams of BPF powder, with particle sizes ranging from 180 to 250 μm and a moisture content below 0.05 kg H_2O/kg BPF solids, were placed in open glass containers. Three replicate samples of each powder were individually sealed in separate humidity chambers containing a NaCl saturated solution, which maintained a relative humidity of 75.5%, and stored at 25 °C for 7 days. The samples were initially prepared at 20 °C. Hygroscopicity (HG), defined as the percentage of moisture adsorbed per 100 g of dry solids (g/100 g), was calculated using Eq. 8 (Sablani *et al.* 2008),

$$\text{HG} = (\Delta M / (M + M_i)) / (1 + \Delta M / M) \tag{8}$$

where D_m (g) represents the increase in the powder's weight after reaching equilibrium, M is the initial mass (g) of the powder, and M_i (% wb) is the free water content of the powder before exposure to the humid air environment.

Bioactive Properties

Determination of total anthocyanin content

The total anthocyanin content (TAC) of the samples was determined using the pH differential method, a commonly employed technique for quantifying anthocyanins. The TAC was expressed as cyanidin-3-glucoside equivalents, a standard reference compound for anthocyanin analysis. The TAC calculation was carried out using Eq. 9, which is adapted from (Maran *et al.* 2015),

$$\text{Anthocyanin content}\left(\frac{\text{mg}}{\text{L}}\right) = \frac{A \times \text{MW} \times \text{DF} \times V \times 1000}{a \times l \times m} \qquad (9)$$

where A represents the absorbance of the sample at specific wavelengths as measured by the pH differential method, MW is the molecular weight of cyanidin-3-glucoside, which is 449.2 g/mol, DF denotes the dilution factor of the sample, V is the volume of solvent used in millilitres (mL), a is the molar absorptivity coefficient of cyanidin-3-glucoside, which is 26,900 $L \cdot mol^{-1}cm^{-1}$, and l is the path length of the cell, typically 1 cm.

To minimize interference from impurities or other compounds, all extracts were filtered through Whatman No. 1 filter paper prior to analysis. The pH differential method is recognized for its specificity in measuring monomeric anthocyanins, as compounds that do not exhibit a reversible structural transformation between pH 1.0 and 4.5 do not interfere significantly with absorbance measurements. It is assumed that any potential interfering substances absorbing at 520 nm and 700 nm were either absent or present in negligible amounts. This approach has been validated in previous studies as sufficiently robust for plant-based extracts.

Total phenolic content

The total phenolic content (TPC) of the BPF powder was assessed using the Folin-Ciocalteu method. In this procedure, 200 µL of the sample was combined with 1720 µL of distilled water, followed by the addition of 80 µL of Folin-Ciocalteu reagent. After thorough mixing, 200 µL of 20% Na_2CO_3 was added, and the final volume was adjusted to 4 mL with an additional 1800 µL of water. The absorbance of each sample was then measured at 725 nm using a ultraviolet-visible (UV-VIS) spectrophotometer (Shimadzu Corporation, Kyoto, Japan). Gallic acid served as the standard, and the total phenolic content was determined from a calibration curve of gallic acid, with results expressed as gallic acid equivalents (GAE).

Structural and Morphological Properties

X-ray diffraction (XRD) analysis of BPF powder

To evaluate the crystallinity and structural features of BPF powder of various sizes, an X-ray diffractometer (D8 Advance, Bruker, Germany) was used. The instrument was operated at 40 kV and 40 mA, utilizing an Analytical X-ray B.V. powder X-ray diffractometer with a wavelength of 1.54 Å (Cu Kα radiation). The sample was mounted on a stub, and diffraction data were collected over a 2θ range of 5 to 70° at a scan rate of 5°/min, following the method of Hunter *et al.* (2011). This procedure was conducted in triplicate to ensure accuracy and reproducibility of the results.

Fourier-transform infrared spectroscopy

Fourier transform infrared (FTIR) spectroscopy (FTIR/NIR 400, Perkin–Elmer Inc., Hillsboro, OR, USA) was used to identify the organic functional groups in the BPF powder samples. The samples were placed on an attenuated total reflection (ATR) plate, and spectra were collected from four scans within the spectral range of 4000 to 400 cm^{-1}. The FTIR spectroscopy detects changes in the functional groups of metabolites by analysing specific infrared peaks, which indicate alterations in the chemical composition of the BPF samples.

Scanning electron microscopy analysis of BPF powder

The morphological characteristics of the BPF were analysed using a scanning electron microscope (SEM) (Model: Evo18, Carl Zeiss, Oberkochen, Germany) coupled with energy dispersive X-ray spectroscopy (EDX) (Model: Quantax 200 with X-Flash 6130; Bruker, Karlsrushe, Germany). Prior to SEM analysis, the samples were gold-coated (Quorum Technologies, Laughton, UK) to enhance imaging quality.

Statistical Analyses

An analysis of variance (ANOVA) and t-tests were employed to assess the mean differences, with significance determined at $p < 0.05$ and a 95% confidence level. The average values of all experimental data were analyzed using statistical parameters, including Root Mean Square Error (RMSE) and the coefficient of determination (R^2), which were calculated using Eqs. 10 and 11:

$$RMSE = \sqrt{\frac{\sum_{i=1}^{N}(EV-MV)^2}{N}} \tag{10}$$

$$R^2 = 1 - \frac{\sum_{i=1}^{N}(MV-EV)^2}{\sum_{i=1}^{N}(EV-EV_{avg})^2} \tag{11}$$

where EV is the experimental value, MV is the modelled value, EV_{avg} is the average of the experimental value, and *N* is the number of observations.

RESULTS AND DISCUSSION

Density Measurements of BPF Powders

Density measurements are crucial for understanding the physical properties of powdered food products, influencing their handling, processing, and application. In the analyzed samples of BPF powder, Sample C, which was dried at 70 °C, exhibited the highest bulk density at 1.44 g/mL (Table 2). This indicates a more compact particle packing relative to other samples, even without external compaction. Comparable findings are reported by Hunter *et al*. (2011), who observed that thermal processing can increase the bulk density of food powders by enhancing particle compaction. Tapped density, which typically exceeds bulk density due to compaction, was relatively uniform across the samples, with both Sample A and Sample D achieving a tapped density of 1.4 g/mL. Particle density, representing the true density of the particles excluding voids, ranged from 1.48 g/mL in Sample B to 1.55 g/mL in Sample D. Sample D, obtained from natural sun-drying, demonstrated the highest particle density, reflecting the densest particles among

the samples. Conversely, Sample B exhibited a lower particle density, indicating slightly less dense particles.

Table 2. Density Measurements of BPF Powders

Sample	Bulk Density (g/mL)	Tapped Density (g/mL)	Particle Density (g/mL)
A	1.31 ±0.2[c]	1.4 ± 0.3[c]	1.48 ± 0.7[d]
B	1.27 ± 0.5[d]	1.33 ± 0.5[d]	1.48 ± 0.8[c]
C	1.44 ± 0.9[b]	1.40 ± 0.8[a]	1.51 ± 0.7[b]
D	1.40 ± 0.5[a]	1.40 ± 0.3[b]	1.55 ± 0.3[a]

Note: Values are expressed as mean ± standard deviation (SD) based on three independent replicates (n = 3). Different superscript letters within a column denote significant differences ($p < 0.05$). Alpha level (α) = 0.05 was used for determining statistical significance.

Hausner Ratio and Porosity of BPF Powders

The Hausner ratio, calculated as the ratio of tapped density to bulk density, serves as a crucial measure of powder flowability. A Hausner ratio close to 1 typically signifies good flow properties, indicating that the powder flows smoothly with minimal friction. In this study, Sample C, dried at 70 °C, had a Hausner ratio of 0.97, suggesting excellent flowability and suitability for applications requiring efficient powder handling (Table 3). Conversely, Sample A, dried at 50 °C, had a Hausner ratio of 1.07, indicating relatively poorer flow properties. This higher ratio may be due to increased particle friction and reduced compaction efficiency, which can impede smooth powder flow, as observed in other food powder studies (Szulc and Lenart 2016).

Porosity, which measures the fraction of void space within the powder, provides additional insights into its structural characteristics. Lower porosity percentages indicate a denser, more compact powder. In this study, Samples A and C exhibited low porosities of 6.14% and 7.86%, respectively, reflecting a compact structure with minimal voids. Conversely, Sample B had a higher porosity of 11.28%, suggesting more void space between particles, which may affect its structural integrity and performance in applications requiring dense powder forms. This aligns with findings from similar research, where higher porosity can impact the powder's flow and structural stability (Roongruangsri and Bronlund 2016).

Table 3. Flowability and Porosity of BPF Powders

Sample	Hausner Ratio	Porosity (%)
A	1.06 ± 0.2[a]	6 ± 0.2[d]
B	1.04 ± 0.5[b]	11 ± 0.2[a]
C	0.97 ± 0.7[d]	7 ± 0.08[c]
D	1.00 ± 0.6[c]	10 ± 0.07[b]

Note: Values are expressed as mean ± standard deviation (SD), based on three replicates (n = 3). Different superscript letters within each column denote significant differences ($p < 0.05$). The significance level was set at α = 0.05.

Hydration and Adsorption Properties

The WSI quantifies the proportion of a powder that dissolves in water, reflecting its ease of integration into liquid solutions. In this study, Sample C, which was dried at 70 °C, exhibited the highest WSI at 0.84% (Table 4). This elevated solubility indicated that Sample C integrated rapidly into liquid solutions, making it particularly suitable for

applications where quick dissolution is required, a characteristic that aligns with findings in similar food powder research (Santhalakshmy *et al.* 2015).

The Water Holding Capacity (WHC) measures a powder's ability to retain water, which is crucial for the texture and stability of food products. Sample D, which was sun-dried, showed the highest WHC at 5.6 g/g, demonstrating superior water retention relative to its weight. This enhanced WHC is advantageous for maintaining moisture levels in final products, as seen in other studies that highlight the importance of water retention for product stability (Jongaroontaprangsee *et al.* 2007). In contrast, Sample A, dried at 50 °C, had a lower WHC of 2 g/g, indicating reduced moisture retention capabilities. This lower WHC suggests that Sample A may have been less effective in applications where maintaining moisture is critical.

Table 4. Hydration and Adsorption Properties of BPF Powders

Sample	WSI (%)	WHC (g/g)
A	0.46 ± 0.3[d]	2.00 ± 0.7[d]
B	0.72 ± 0.6[b]	2.52 ± 0.8[c]
C	0.84 ± 0.3[a]	3.18 ± 0.5[b]
D	0.49 ± 0.6[c]	5.6 ± 0.8[a]

Notes: Values are expressed as mean ± standard deviation (SD), based on three replicates (n = 3). Different superscript letters within each column denote significant differences ($p < 0.05$). The significance level was set at $\alpha = 0.05$.

Solubility Time and Hygroscopicity Levels of Powdered BPF

The solubility and hygroscopicity of BPF powder were systematically analyzed, revealing dissolution times ranging from 148 to 162 s (Table 5). Despite this variation, statistical analysis showed no significant differences in solubility among the samples ($p > 0.05$). Specifically, lower moisture content enhances solubility, as noted by Caliskan and Dirim (2016), who observed that removing excess moisture typically improves powder solubility.

Table 5. Soluble Time and Hygroscopicity Levels, TPC and Anthocyanin Content of Powdered BPF

Sample	Late Time (s)	Hygroscopicity Levels (%)	TPC (mgGAE/g dwb)	Anthocyanin (mg/g dwb)
A	158 ± 0.18[b]	11.75 ± 0.09[c]	64.58 ± 0.02[c]	1.62 ± 0.10[a]
B	150 ± 0.15[c]	12.12 ± 0.5[b]	65.15 ± 0.13[c]	1.85 ± 0.03[b]
C	148 ± 0.13[d]	12.79 ± 0.6[a]	67.25 ± 0.09[b]	2.03 ± 0.05[b]
D	162 ± 0.18[a]	11.25 ± 0.8[d]	68 ± 0.08[a]	2.38 ± 0.06[a]

Notes: Values are expressed as mean ± standard deviation (SD), based on three replicates (n = 3). Different superscript letters within each column denote significant differences ($p < 0.05$). The significance level was set at $\alpha = 0.05$.

In this study, Sample C exhibited the shortest solubility time of 148 s and the highest hygroscopicity level of 12.79%, suggesting a strong moisture absorption capacity that might contribute to its faster dissolution rate. Conversely, Sample D, which had the longest solubility time of 162 s, showed the lowest hygroscopicity level at 11.25%, indicating a reduced tendency to absorb moisture and potentially contributing to its slower dissolution. Samples A and B had solubility times of 158 and 150 s, respectively, with corresponding hygroscopicity levels of 11.75% and 12.12%. This variability in

hygroscopicity among the samples is likely due to differences in factors, such as particle size, surface area, and processing methods, supported by Agustini (2018), who noted the significant effects of these parameters on moisture absorption and solubility. Despite the observed variations in hygroscopicity, the solubility of the BPF powder remained stable across the samples. This stability may be attributed to controlled processing conditions, including uniform drying techniques and consistent particle size distribution, which help maintain solubility despite differences in hygroscopicity.

TPC and Anthocyanin Content in the BPF Powders

The study assessed variations in total phenolic content (TPC) and anthocyanin levels in BPF samples subjected to different drying conditions (Table 5). An overall increase in TPC and anthocyanin content was observed with higher oven drying temperatures; however, the sun-dried sample (Sample D) exhibited the highest values. This suggests that, in addition to temperature, other factors such as prolonged drying duration, exposure to natural light, and enzymatic activity may significantly influence the retention or enhancement of these bioactive compounds. Specifically, Sample A (50 °C) recorded a TPC of 64.58 mg GAE/g dry weight (dwb) and an anthocyanin content of 1.62 mg/g dwb. Sample B (60 °C) showed a modest increase, with a TPC of 65.15 mg GAE/g dwb and anthocyanin content of 1.85 mg/g dwb. Sample C (70 °C) exhibited further enhancement, with a TPC of 67.25 mg GAE/g dwb and anthocyanin content of 2.03 mg/g dwb. Notably, Sample D, which was sun-dried, recorded the highest concentrations, with a TPC of 68.00 mg GAE/g dwb and anthocyanin level of 2.38 mg/g dwb.

The observed increase in TPC and anthocyanin levels with higher drying temperatures can be attributed to the effect of temperature on the stabilization and concentration of these compounds. Higher temperatures tend to reduce moisture content more efficiently, which can lead to a more concentrated product. Additionally, thermal processing can activate certain enzymatic reactions that enhance the extraction of phenolic compounds and anthocyanins, albeit without significant degradation. These findings align with previous research indicating that different types of drying can better preserve and enhance bioactive compounds in BPF (Hariadi *et al.* 2024). The increased concentrations observed in Sample D may also reflect the effective preservation of these compounds through sun-drying, which prevents excessive heat-induced degradation while promoting compound stability.

SEM Analysis

The SEM analysis of BPF powders, subjected to different drying conditions, provides a comprehensive view of their microstructural changes across magnifications of 250 X and 2.50 KX (Fig. 2). These combined magnifications offer insights into both the overall morphology and finer structural details of the samples. At lower magnification (250 X), the SEM images reveal general particle distribution and surface texture across the samples. As the magnification increases to 2.50 KX, more intricate details, such as surface roughness, porosity, and the degree of particle fragmentation, become evident. In Sample A (50 °C), the combined analysis shows smooth surfaces with minimal roughness and a lack of significant porosity, even at higher magnification, indicating that low-temperature drying effectively preserved the structural integrity of the BPF particles. Sample B (60 °C) demonstrates an increase in surface roughness and the beginnings of micro-cracking, which became more pronounced at 2.50 KX, reflecting the onset of thermal-induced stress.
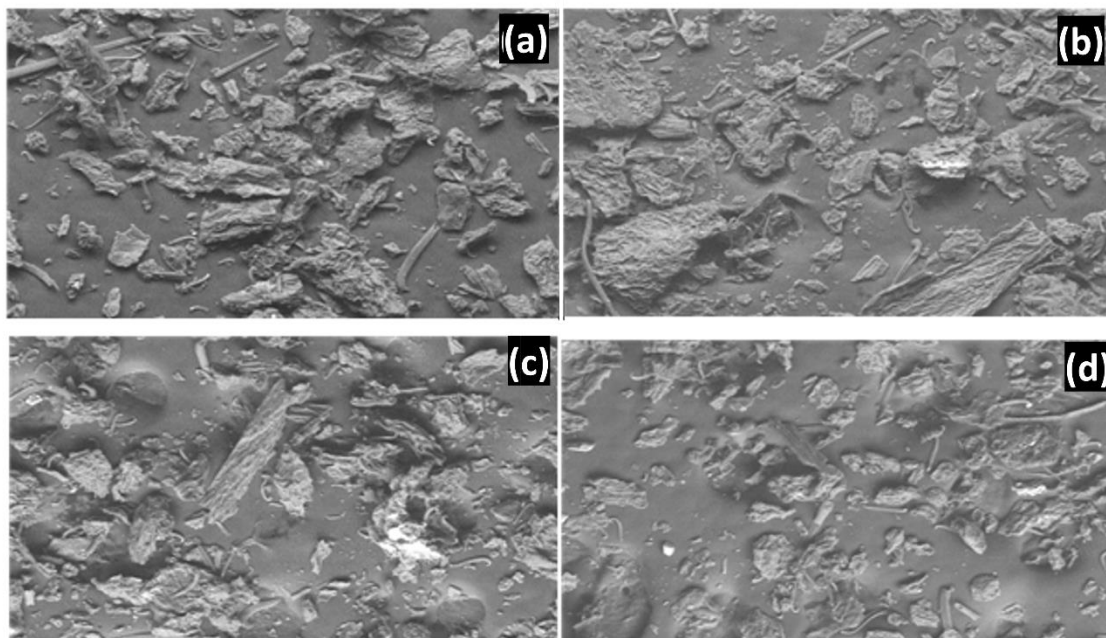
bioresources.cnr.ncsu.edu

Fig. 2. SEM images of BPF powder of (a) Sample A, (b) Sample B, (c) Sample C, and (d) Sample D at magnification of 250 X

Sample C (70 °C) presents the most significant structural alterations; at 250 X, the particles appear more fragmented, and at 2.50 KX, the extensive porosity and surface disintegration are visible, indicating that higher temperatures led to considerable degradation of the particle structure. Sample D (sun-dried) displays large, irregular particles with a coarse texture at 250 X, while at 2.50 KX, the uneven surface with large pores and significant cracking highlights the variability and less controlled nature of sun drying, resulting in a more heterogeneous microstructure (Caparino *et al.* 2012; Burgain *et al.* 2017). The study observed that higher drying temperatures resulted in more pronounced particle disintegration and greater surface area exposure, which were clearly visible at higher SEM magnifications (2.50 KX). These structural changes directly correlated with alterations in physical properties like flowability and solubility, mirroring the results observed in the BPF powders in this study. The progression from smooth, intact particles at lower drying temperatures to highly fragmented, porous structures at higher temperatures or with natural sun drying reveals the delicate balance between drying efficiency and the preservation of the powder's structural integrity. This understanding is crucial for optimizing drying processes to maintain the functional and nutritional properties of BPF in various applications.

XRD of Powdered BPF

The crystallinity and structural properties of BPF powder dried at various temperatures were analyzed using XRD (Fig. 3). This analysis is crucial for understanding how different drying temperatures affect the crystallinity and amorphous content of the powder, which in turn influences its stability, solubility, and bioavailability of natural compounds.
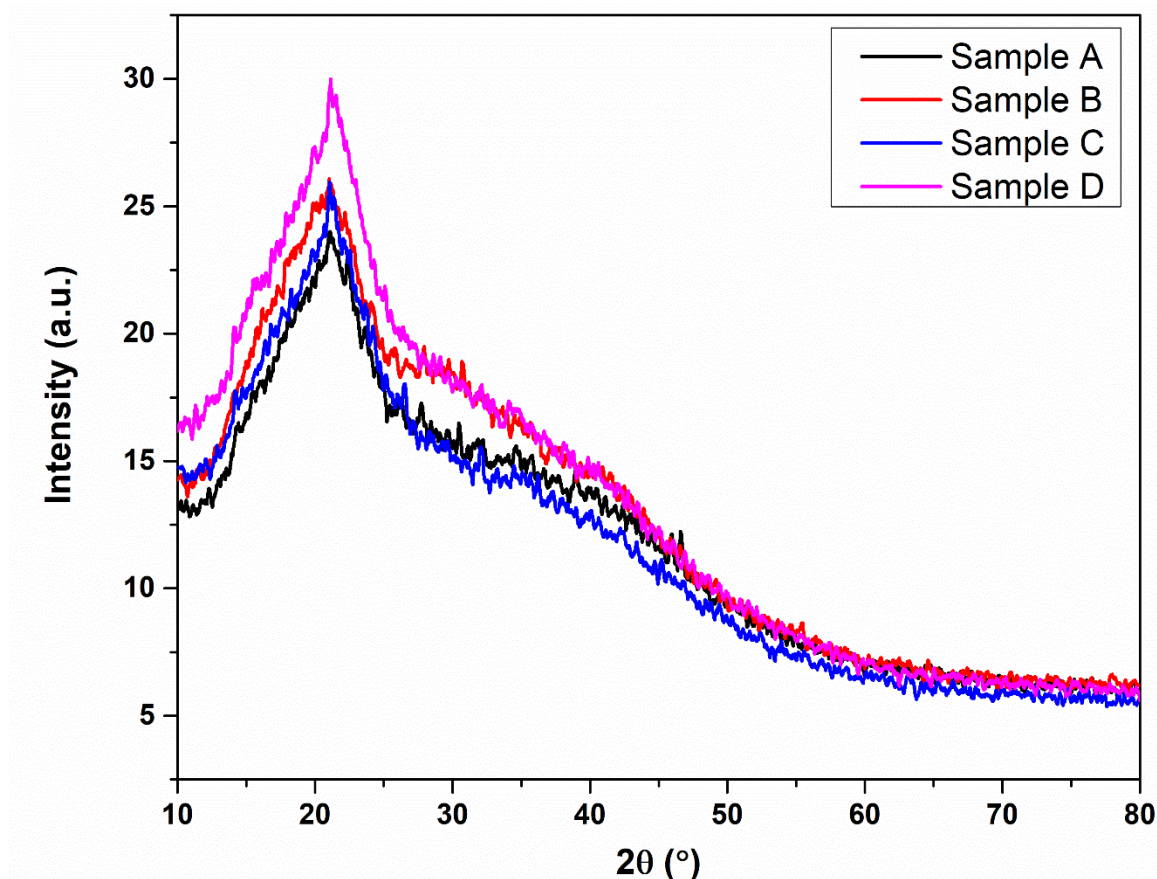
Fig. 3. XRD patterns of BPF powder of Sample A, B, C and D

Sample A, dried at 50 °C, displayed an XRD pattern with a diffraction angle of 30.505°, a d-spacing of 2.928 Å, a net intensity of 56.7, and a gross intensity of 540. The crystallinity of this sample was measured at 22.2%, with an amorphous content of 77.8% (Table 6). These findings are consistent with literature suggesting that moderate drying temperatures partially preserve crystalline regions while maintaining a significant proportion of amorphous content. **Sample B**, dried at 60 °C, showed a slightly higher diffraction angle of 30.739° and a reduced d-spacing of 2.906 Å, with a net intensity of 60.6 and a gross intensity of 610. The crystallinity decreased to 19.3%, while the amorphous content increased to 80.7%. This indicates that higher drying temperatures enhance the amorphous nature of the material, as reported in previous studies that found increased amorphous content with higher processing temperatures due to disruption of crystalline structures (Purohit *et al.* 2019).

Sample C, dried at 70 °C, exhibited a diffraction angle of 21.041° and a larger d-spacing of 4.218 Å (Table 6). This sample had a net intensity of 238 and a gross intensity of 860, with 100% relative intensity. The crystallinity was the highest among all samples at 26.3%, while the amorphous content was 73.7%. The higher crystallinity observed at elevated drying temperatures may result from the recrystallization of certain compounds, a phenomenon documented in studies where thermal treatment led to the reorganization of molecular structures into more ordered forms (Caparino *et al.* 2012).

Sample D, which was naturally dried under the sun, had a diffraction angle of 38.079° and a d-spacing of 2.361 Å. The net intensity was 72.1, with a gross intensity of 545. The crystallinity was measured at 21.9%, with 78.1% amorphous content. The higher

amorphous content observed in sun-dried samples is typical due to the slower drying process, which allows less structural rearrangement compared to thermal drying. The XRD analysis reveals that drying temperature significantly influences the crystallinity and amorphous content of BPF powder. **Sample C**, dried at 70 °C, exhibited the highest crystallinity, suggesting that higher temperatures promote the formation of crystalline structures. In contrast, lower temperatures and natural drying methods result in higher amorphous content. These results align with previous studies indicating that higher drying temperatures facilitate the reorganization of molecular structures into more ordered forms, while lower temperatures or slower drying methods preserve amorphous regions (Ho *et al.* 2017).

Table 6. Crystallinity and Amorphous Properties of Powdered BPF

Sample	Angle	d Value	Net Intensity	Gross intensity	Rel. intensity	Crystallinity (%)	Amorphous (%)
A	30.505	2.928	56.7	540	100%	22.2	77.8
B	30.739	2.906	60.6	610	100%	19.3	80.7
C	21.041	4.218	238	860	100%	26.3	73.7
D	38.079	2.361	72.1	545	100%	21.9	78.1

FTIR Analysis

The FTIR analysis of BPF samples dried under varying conditions (Samples A, B, C, and D) provides a comprehensive understanding of their chemical composition and the stability of functional groups across different drying methods (Fig. 4). Sample A, dried at 50 ºC, revealed a rich chemical profile, including aromatic rings (1,2,3-trisubstituted and 1,4-disubstituted), sulfoxides, alkyl aryl ethers, alcohols, and conjugated alkenes, with significant hydrogen bonding indicated by a broad O-H stretching peak (Table 7(a)). As the drying temperature increased to 60 ºC in Sample B, the FTIR spectrum remained largely consistent with Sample A, preserving the same key functional groups, while also introducing additional features like alkynes and free alcohols (Table 7(b)).

Table 7(a). FTIR Data of BPF Powder (Sample A)

Peak	Intensity	Appearance	Group	Compound Class
428.20	96.84	--------	--------	--------
590.22	85.33	--------	--------	-------
777.31	96.29	Strong	C-H bonding	1,2,3-trisubstituted
821.68	96.93	Strong	C-H bonding	1,4-Disubstituted
1060.85	58.71	Strong	S=O stretching	Sulfoxide
1244.09	93.81	Strong	C-O stretching	Alkyl aryl ether
1417.68	85.06	Medium	O=H bonding	Alcohol
1639.49	52.75	Medium	C=C stretching	Conjugated Alkene
3421.72	10.00	Strong Broad	O-H stretching	Alcohol

Table 7(b). FTIR Data of BPF Powder (Sample B)

Peak	Intensity	Appearance	Group	Compound Class
424.34	97.67	-------	---------	------------
617.22	82.94	--------	---------	----------
777.31	94.64	Strong	C-H bonding	1,2,3-trisubstituted
821.68	95.89	Strong	C-H bonding	1,4-Disubstituted
1060.85	45.17	Strong	S=O stretching	Sulfoxide
1242.16	92.41	Strong	C-O stretching	Alkyl aryl ether
1415.75	76.72	-------	---------	------------
1641.42	41.09	Strong	C=C stretching	Alkene
2113.98	97.38	Weak	C=C stretching	Alkyne
3408.22	10.00	-------	---------	------------
3743.83	97.49	Medium	O-H stretching	Alcohol Free

Table 7(c). FTIR Data of BPF Powder (Sample C)

Peak	Intensity	Appearance	Group	Compound Class
617.22	72.62	-------	---------	------------
777.31	93.61	Strong	C-H bonding	1,2,3-Trisubstituted
821.68	94.93	Strong	C-H bonding	1,4-Disubstituted
1058.92	28.39	Strong	S=O stretching	Sulfoxide
1246.02	88.89	Strong	C-O stretching	Alkyl aryl ether
1415.75	68.49	Medium	O-H bonding	Alcohol
1641.42	27.33	Medium	C=C stretching	Conjugated Alkene
2133.27	96.97	Strong	N=C=N stretching	Carbodiimide
2924.09	76.39	Medium	C-H stretching	Alkane
3423.65	10.00	Strong	O-H stretching	Alcohol

Table 7(d). FTIR Data of BPF Powder (Sample D)

Peak	Intensity	Appearance	Group	Compound Class
542.00	61.73	-------	---------	------------
777.31	91.79	Strong	C-H bonding	1,2,3-trisubstituted
821.68	93.57	Strong	C-H bonding	1,4-Disubstituted
1060.85	24.25	Strong	S=O stretching	Sulfoxide
1242.16	85.32	Strong	C-O stretching	Alkyl aryl ether
1317.38	93.78	Medium	O-H bonding	Phenol
1419.61	68.57	Medium	O-H bonding	Alcohol
1651.07	20.47	Medium	C=C stretching	Alkene
2133.27	94.71	Strong	N=C=N stretching	Carbodiimide
2922.16	62.95	Medium	C-H stretching	Alkane

bioresources.cnr.ncsu.edu

Sample C, dried at 70 ºC (Table 7(c)), continued to exhibit stability in the chemical structure, with notable peaks for aromatic rings, sulfoxides, and alkyl aryl ethers, although there was a slight reduction in sulfoxide intensity and the appearance of carbodiimides, suggesting some changes in chemical composition at higher temperatures (Baltacıoğlu *et al.* 2024). Finally, Sample D, which was dried naturally under the sun, displayed a chemical profile similar to the thermally dried samples, with preserved aromatic rings, sulfoxides, and alkyl aryl ethers, but with the unique presence of phenolic compounds, which are known for their antioxidant properties (Table 7(d)). The analysis indicates that the key bioactive components of BPFs were largely stable across different drying methods, with natural sun drying showing a comparable preservation of chemical constituents, including the retention of phenols, which are less prominent in thermally dried samples. This suggests that both thermal and natural drying methods effectively maintained the bioactive potential of BPFs, with minor variations in specific functional groups depending on the drying conditions (Reddy *et al.* 2024).
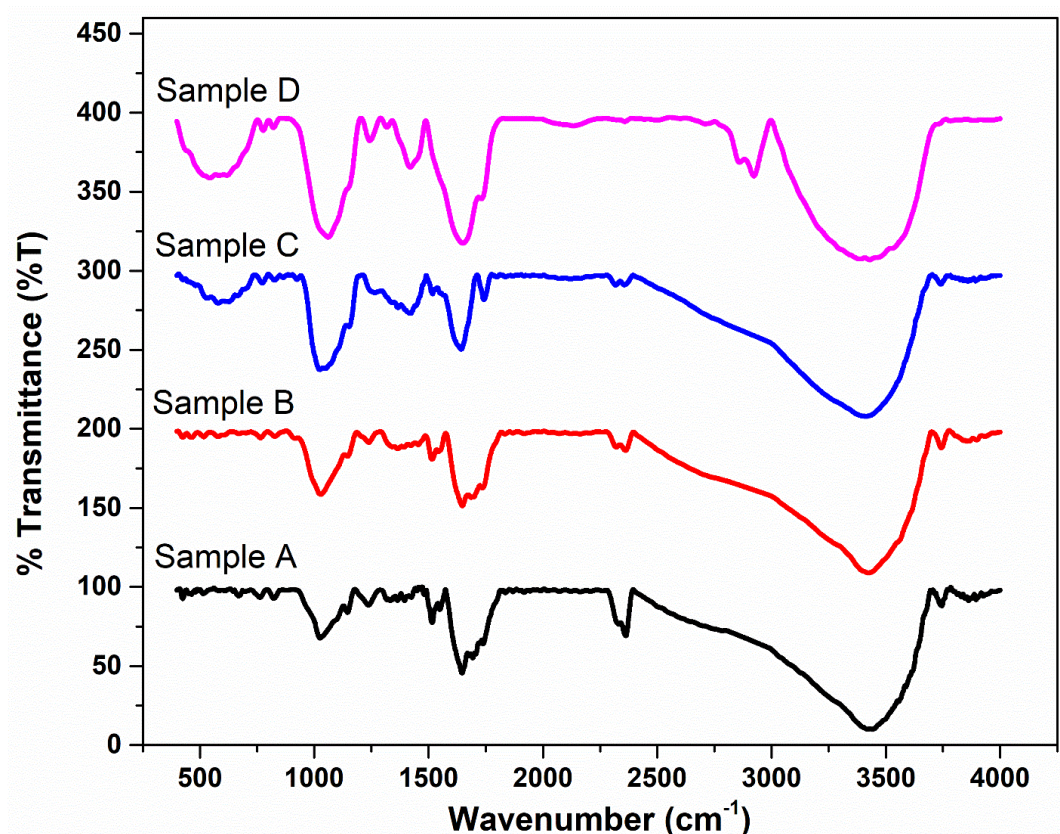

Fig. 4. FTIR spectra of Sample A, Sample B, Sample C, and Sample D

CONCLUSIONS

This study systematically investigated the effects of various drying conditions on the properties of butterfly pea flower (BPF) powder, offering a comprehensive understanding of how these methods influence solubility, physical characteristics, and chemical composition.

1. The solubility of BPF powder was consistent across different drying temperatures, ranging from 148 to 162 s, indicating that solubility is largely unaffected by the drying method.

2. Sample C, dried at 70 °C, exhibited the fastest solubility and highest hygroscopicity, suggesting that increased drying temperatures enhance moisture absorption, potentially accelerating dissolution.

3. The total phenolic content (TPC) and anthocyanin levels showed a positive correlation with drying temperature, with Sample D, from sun-drying, exhibiting the highest concentrations of these bioactive compounds. This trend supports the notion that higher drying temperatures can both preserve and enhance the bioactive properties of BPF powder.

4. Density measurements revealed that Sample C, with its higher bulk density and lower Hausner Ratio, demonstrated superior compaction and flowability, which is essential for processing and application.

5. The scanning electron microscope (SEM) analysis highlighted that higher drying temperatures induce more significant morphological changes, including increased porosity and fragmentation, with Sample C showing the most pronounced alterations.

6. Sample A, dried at 50 °C, maintained a smoother surface, while sun-dried Sample D displayed coarser particles.

7. The X-ray diffraction (XRD) analysis confirmed that higher temperatures promote crystallinity, with Sample C achieving the highest crystallinity and lowest amorphous content, aligning with the observed increase in bioactive compounds.

8. The Fourier transform infrared (FTIR) analysis indicated that key functional groups were well-preserved across drying methods, with sun-drying retaining notable levels of phenolic compounds.

9. Overall, drying conditions significantly influenced the solubility, structure, and bioactive content of BPF powder, offering practical insights for optimizing drying strategies in food and nutraceutical applications.

REFERENCES CITED

Agustini, S. (2018). "The characterization of mango (*Mangifera indica* L.) powder of various drying temperature," *J. Phys. Conf. Ser.* 1095, article ID 12035. DOI: 10.1088/1742-6596/1095/1/012035

Archana Shenoy, H., and Prakash, J. (2002). "Wheat bran (*Triticum aestivum*): Composition, functionality and incorporation in unleavened bread," *J. Food Qual.* 25, 197-211. DOI: 10.1111/j.1745-4557.2002.tb01019.x

Baltacıoğlu, C., Keskin, O., Baltacıoğlu, H., and Ağçam, E. (2024). "Encapsulation and drying methods in the production of powdered red cabbage (*Brassica oleracea* L.): Chemometrics and Fourier transform infrared spectroscopy," *Food Sci. Technol. Int.* Article ID 10820132241238260. DOI: 10.1177/1082013224123826

Barman, P., and Kar, S. (2023). "*Clitoria ternatea*: A low-cost noble blue tea in India," *J. Surv. Fish Sci.* 10(1S), 6128-6138.

Belwal, T., Cravotto, C., Prieto, M. A., Venskutonis, P. R., Daglia, M., Devkota, H. P., Baldi, A., Ezzat, S. M., Gómez-Gómez, L., Salama, M. M., *et al.* (2022). "Effects of different drying techniques on the quality and bioactive compounds of plant-based products: A critical review on current trends," *Dry. Technol.* 40(8), 1539-1561. DOI: 10.1080/07373937.2022.2068028

Burgain, J., Petit, J., Scher, J., Rasch, R., Bhandari, B., and Gaiani, C. (2017). "Surface chemistry and microscopy of food powders," *Prog. Surf. Sci.* 92(4), 409-429. DOI: 10.1016/j.progsurf.2017.07.002

Caliskan, G., and Dirim, S. N. (2016). "The effect of different drying processes and the amounts of maltodextrin addition on the powder properties of sumac extract powders," *Powder Technol.* 287, 308-314. DOI: 10.1016/j.powtec.2015.10.019

Caparino, O. A., Tang, J., Nindo, C. I., Sablani, S. S., Powers, J. R., and Fellman, J. K. (2012). "Effect of drying methods on the physical properties and microstructures of mango (Philippine 'Carabao' var.) powder," *J. Food Eng.* 111(1), 135-148.

Chuchird, P., Pattarathitiwat, P., and Pongprajak, A. (2024). "Formulation and evaluation of physical, chemical and sensory properties of instant functional beverage powder containing Pathum Thani fragrance rice, soy protein and milk powder," *Food Res.* 8(3), 394-401. DOI: 10.26656/fr.2017.8(3).319

Enaru, B., Drețcanu, G., Pop, T. D., Stănilă, A., and Diaconeasa, Z. (2021). "Anthocyanins: Factors affecting their stability and degradation," *Antioxidants* 10(12), article 1967. DOI: 10.3390/antiox10121967

Ho, T. M., Truong, T., and Bhandari, B. R. (2017). "Methods to characterize the structure of food powders – A review," *Biosci. Biotechnol. Biochem.* 81(4), 651-671. DOI: 10.1080/09168451.2016.1274643

Hunter, M. S., DePonte, D. P., Shapiro, D. A., Kirian, R. A., Wang, X., Starodub, D., Marchesini, S., Weierstall, U., Doak, R. B., Spence, J. C. H., *et al.* (2011). "X-ray diffraction from membrane protein nanocrystals," *Biophys. J.* 100(1), 198-206. DOI: 10.1016/j.bpj.2010.10.049

Jinapong, N., Suphantharika, M., and Jamnong, P. (2008). "Production of instant soymilk powders by ultrafiltration, spray drying and fluidized bed agglomeration," *J. Food Eng.* 84(2), 194-205. DOI: 10.1016/j.jfoodeng.2007.04.032

Jongaroontaprangsee, S., Tritrong, W., Chokanaporn, W., Methacanon, P., Devahastin, S., and Chiewchan, N. (2007). "Effects of drying temperature and particle size on hydration properties of dietary fiber powder from lime and cabbage by-products," *Int. J. Food Prop.* 10(4), 887-897. DOI: 10.1080/10942910601183619

Kadam, D. M., Wilson, R. A., Kaur, S., and Manisha. (2012). "Influence of foam mat drying on quality of tomato powder," *Int. J. Food Prop.* 15(1), 211-220. DOI: 10.1080/10942911003763701

Maran, J. P., Sivakumar, V., Thirugnanasambandham, K., and Sridhar, R. (2014). "Extraction of natural anthocyanin and colors from pulp of jamun fruit," *J. Food Sci. Technol.* 52, 3617-3626. DOI: 10.1007/s13197-014-1429-0

Marpaung, A. M., Lee, M., and Kartawiria, I. S. (2020). "The development of butterfly pea (*Clitoria ternatea*) flower powder drink by co-crystallization," *Indones. Food Sci. Technol. J.* 3(2), 34-37. DOI: 10.22437/ifstj.v3i2.10185

Oguis, G. K., Gilding, E. K., Jackson, M. A., and Craik, D. J. (2019). "Butterfly pea (*Clitoria ternatea*), a cyclotide-bearing plant with applications in agriculture and medicine," *Front. Plant Sci.* 10, article 645. DOI: 10.3389/fpls.2019.00645

Purohit, S. R., Jayachandran, L. E., Raj, A. S., Nayak, D., and Rao, P. S. (2019). "X-ray diffraction for food quality evaluation," in: *Evaluation Technologies for Food Quality*, Woodhead Publishing, Sawston, UK, pp. 579–594. DOI: 10.1016/B978-0-12-814217-2.00022-6

Reddy Keerthi, B., Meena, S., Brath Gautam, P., Kumar Meena, K., and Chandra Rai, D. (2024). "Optical, thermal, FTIR, SEM-EDX and 1H NMR analysis of *Chenopodium album* (Bathua) powder prepared using different drying techniques," *Microchem. J.* 201, article ID 110537. DOI: 10.1016/j.microc.2024.110537

Roongruangsri, W., and Bronlund, J. E. (2016). "Effect of air-drying temperature on physico-chemical, powder properties and sorption characteristics of pumpkin powders," *Int. Food Res. J.* 23(3), 962-972.

Sablani, S. S., Shrestha, A. K., and Bhandari, B. R. (2008). "A new method of producing date powder granules: Physicochemical characteristics of powder," *J. Food Eng.* 87(3), 416-421. DOI: 10.1016/j.jfoodeng.2007.12.024

Santhalakshmy, S., Don Bosco, S. J., Francis, S., and Sabeena, M. (2015). "Effect of inlet temperature on physicochemical properties of spray-dried jamun fruit juice powder," *Powder Technol.* 274, 37-43. DOI: 10.1016/j.powtec.2015.01.016

Szulc, K., and Lenart, A. (2016). "Effect of composition on physical properties of food powders," *Int. Agrophys.* 30(2), 237-243. DOI: 10.1515/intag-2015-0084

Thamkaew, G., Sjöholm, I., and Galindo, F. G. (2021). "A review of drying methods for improving the quality of dried herbs," *Crit. Rev. Food Sci. Nutr.* 61(11), 1763-1786. DOI: 10.1080/10408398.2020.1765309

Vidana Gamage, G. C., Lim, Y. Y., and Choo, W. S. (2021). "Anthocyanins from *Clitoria ternatea* flower: Biosynthesis, extraction, stability, antioxidant activity, and applications," *Front. Plant Sci.* 12, article ID 792303. DOI: 10.3389/fpls.2021.792303

Yağcı, S., and Göğüş, F. (2008). "Response surface methodology for evaluation of physical and functional properties of extruded snack foods developed from food-by-products," *J. Food Eng.* 86(1), 122-132. DOI: 10.1016/j.jfoodeng.2007.09.018

Zhang, Z., Song, H., Peng, Z., Luo, Q., Ming, J., and Zhao, G. (2012). "Characterization of stipe and cap powders of mushroom (*Lentinus edodes*) prepared by different grinding methods," *J. Food Eng.* 109(3), 406-413. DOI: 10.1016/j.jfoodeng.2011.11.007

Ziaee, A., O'Connor, E. M., Murphy, E., and O'Reilly, E. (2023). "Spray drying of food," in: *Drying Technology in Food Processing*, Woodhead Publishing, Sawston, UK, pp. 123-155. DOI: 10.1016/B978-0-12-819895-7.00010-9